Cement and Concrete Research 144 (2021) 106417

Contents lists available at ScienceDirect

Cement and Concrete Research

journal homepage: www.elsevier.com/locate/cemconres

Effects of anionic and nonionic surfactants on the dispersion and stability of nanoSiO$_2$ in aqueous and cement pore solutions

Yogiraj Sargam [a], Kejin Wang [a,*], Ayuna Tsyrenova [b], Fei Liu [b], Shan Jiang [b,*]

[a] Iowa State University, Department of Civil, Construction, and Environmental Engineering, Ames, IA 50011, United States of America
[b] Iowa State University, Department of Material Science and Engineering, Ames, IA 50011, United States of America

ARTICLE INFO

Keywords:
Nanosilica
Cement paste
Surfactants
Dispersion
Stability

ABSTRACT

It has been well recognized that the benefits and effectiveness of nanoparticles in cement-based materials could not be maximized if these are not well dispersed. To address this issue, in this study, different anionic (SDS and PCE) and nonionic surfactants (Tweens and Tritons) were used to disperse nanosilica (NS) in aqueous solution and cement pore solution. The results show that the dispersibility of NS in cement pore solution was improved, and the compressive strength of the cement-NS pastes increased linearly with critical micelle concentration (CMC) of nonionic surfactants. Among all surfactants studied, Triton X-405 led the paste to the highest increase in strength (33% at 1-day and 41% at 3-days) since it had the highest CMC. TEM and EDS analysis evidenced that this strength increase might be attributed to the nucleation of outer product CSH gel and its densification with calcite nanocrystals, attributed to Triton X-405 addition.

1. Introduction

Nano-engineering has garnered increasing attention in cement and concrete technology in the last decades. Cement-based composites like concrete can be nano-engineered by the incorporation of various nanosized materials, such as nanoparticles (NP) (zero dimension, 0D), nanofibers (1D), nanoplates/sheets (2D, like graphene), etc. [1]. The nanomaterials can be either blended and embedded into a cement matrix or hybridized onto the surfaces of cement particles, thereby modifying the particle interactions, altering the microstructures, and improving the properties of cement-based materials [1,2]. The benefits of the use of NPs in cement-based materials have been revealed by many researchers [3–9]. They include - (1) facilitating cement hydration by providing nucleation sites for the hydration products to form and grow, (2) improving particle packing of cement matrix and reducing the porosity of mortar/concrete, (3) immobilizing free water in the cementitious system, (4) reducing the porosity of interfacial transition zone (ITZ) between cement paste and aggregate, and (5) consequently enhancing the mechanical properties and durability of concretes. Besides, some NPs also participate in cement hydration. For example, nanosilica (NS) can undergo pozzolanic reaction in a cement matrix, which consumes calcium hydroxide and forms more calcium silicate hydrate (CSH) gel, thus further improving the mechanical properties and durability of concrete [10].

There are several challenges for the use of NPs in cement-based materials, among which uniform dispersion and the cost-to-benefit ratio are key barriers [1]. Despite being produced and supplied in the size of particles below 100 nm, the commercial NP tends to agglomerate and form clusters in the orders of μm in aqueous solutions [11]. The high surface energy and interparticle forces, including van der Waals, hydrogen bonding, and electrostatic interactions, make them highly susceptible to agglomeration [11–13]. When NPs are added to the cementitious system, other factors such as capillary force and interlocking due to particle shape also contribute to their agglomeration [14]. Large, random aggregates not only diminish the benefit of using NPs but also act as potential weak sites for stress concentrations, thereby reducing the mechanical properties of concrete [13]. In this regard, great efforts have been made, and various approaches have been proposed for the dispersion of NPs [4,14–16].

Common approaches to nanoparticle dispersion are through physical methods (e.g., high shear mixing, sonication, milling, etc.) and chemical methods (e.g., use of dispersants, chemical modification of nanoparticle surfaces, etc.). For the cementitious systems, a combination of sonication and surfactant is often suggested. Researchers [12,17–22] have indicated that various surfactants exhibit different efficacy in dispersing nanomaterials. For example, Sindu and Sasmal [20] analyzed five

* Corresponding authors.
E-mail addresses: kejinw@iastate.edu (K. Wang), sjiang1@iastate.edu (S. Jiang).

https://doi.org/10.1016/j.cemconres.2021.106417
Received 13 August 2020; Received in revised form 15 February 2021; Accepted 23 February 2021
Available online 7 March 2021

different surfactants for the dispersion of carbon nanotubes (CNTs) and found that sodium lauryl sulfate (SLSD) exhibited the highest dispersibility whereas that of Triton X-100 was the lowest. Similarly, Liu et al. [22] used CATB (1-hexadecylpyridine bromide), SDS (sodium dodecyl sulfate), and TX 405 (Triton X 405) to disperse CNTs and found that among them, CATB showed the best dispersibility. Kawashima et al. [12] analyzed two superplasticizers (naphthalene and polycarboxylate-based), SC (sodium cholate), SDS, and three variants of nonionic, amphiphilic block copolymers for the dispersion of nano$CaCO_3$ particles, and they found that polycarboxylate (PCE)-based superplasticizer was the most effective surfactant. Some researchers have employed surface modification techniques to facilitate NS particles dispersion [23–25]. They grafted PCE superplasticizer on to the NS particle surfaces to form NS-PCE superplasticizer core-shell NPs (NS@PCE) and found that NS@PCE particles possessed higher stability in saturated calcium hydroxide solution and accelerated cement hydration through deagglomeration [23,24].

Literature review reveals that the dispersion of higher dimensional nanomaterials (e.g., nanofibers, carbon nanotubes, and graphene) has been studied significantly [26–30], while investigations on the use of various surfactants for the dispersion of 0D nanomaterials, or NPs, are still limited [12,14]. Some surfactants that were found effective for dispersion of NPs in aqueous solutions (e.g., SDS and Tween™) have not been widely studied in cement-based materials, and some surfactants that were effective for dispersion of CNTs (e.g., TX-405) have not been applied for dispersion of NPs in cement-based materials yet. Existing technology appears to be insufficient to quantify the dispersion of NPs in the real cementitious matrix. Most quantitative studies on the dispersion of NPs in cement-based materials are conducted in simulated cement solutions, like NaOH and KOH solutions [14,17,22,31]. A few recent studies were conducted on the dispersion of NPs in extracted cement pore solutions [25,32]. It is believed that the dispersion behavior of NPs in extracted cement pore solutions could well simulate the dispersion behavior of the NPs in corresponding cement pastes. However, the understanding of dispersion mechanisms and the dispersant-NP-cement interactions is just the first step.

The present study aims at bridging the above-mentioned research gaps. Its overall objective is to investigate the effects of various surfactants (that have been used by other industries but have not been commonly used in the cement and concrete industry) on the dispersion of NS in cement-based materials. The surfactants studied include two anionic: SDS and PCE-based superplasticizer, and five nonionic: two Tween™ (T20 and T40) and three Triton™ (TX-14, TX-110, and TX-405) surfactants. PCE-based superplasticizer is one of the most commonly used surfactants in cement and concrete materials, and it is used in the present study as a reference. The rest of the surfactants, anionic SDS, and nonionic Tween and Triton groups, are the surfactants commonly used in laboratory detergents [33]. The dispersion and stability of NS suspensions (NS dispersed in aqueous solutions) and cement-NS suspensions (NS dispersed in cement pore solutions) containing these surfactants were evaluated through the measurements of hydrodynamic particle size and zeta potential (ZP) by using dynamic light scattering (DLS), and sedimentation tests. Based on their efficacy, an optimal surfactant (TX405) was selected and further studied for its effect on flowability and early-age compressive strength of cement-NS paste. Its interaction with NS and Portland cement was examined using a transmission electron microscope (TEM) and energy-dispersive spectroscopy (EDS) analyses. Finally, the possible dispersing mechanisms of different types of surfactants were then discussed.

2. Overview of nanoparticle stabilization using surfactants

Depending on the charges of the hydrophilic head in a surfactant molecule, a surfactant is classified as anionic, cationic, zwitterionic (bearing both positive and negative charges), or nonionic (no charges). Surfactants can adsorb at the solid-liquid (S–L) interface to lower the interfacial tension and help disperse and stabilize NPs [34]. The stability of dispersed particles ultimately depends on the interplay of attractive and repulsive forces among particles. As shown in Fig. 1, a stronger repulsive force generally leads to a better-stabilized suspension, while a stronger attractive force often results in particle aggregations. Due to their amphiphilic nature, surfactant molecules adsorb onto the NP surface with their hydrophilic head groups protruding into the solution. Ionic surfactants stabilize NPs by bringing charges to their surface and induce the same charge electrostatic repulsion among the NPs. Differently, nonionic surfactants stabilize NPs via the steric hindrance through the hydration layer at the NP surfaces. The classical DLVO theory suggests that electrostatic repulsion results from the electrical double layers around the electrically charged particles, and the electrical charge stabilization is very sensitive to the ionic strength of the dispersion medium. As the ionic strength increases, the range of the electrostatic repulsion reduces [35]. Cement suspensions generally contain high salt concentration, especially the multi-valency ions, and have high ionic strength. Using anionic surfactant alone may not be able to stabilize NPs in the cementitious system. Nonionic surfactants can provide colloidal stability via the steric hindrance of the hydration layer on the hydrophilic headgroups. This stability is not affected by the surface charge or ionic strength of the solution. This stabilizing mechanism is also most effective in the short-range, which means NPs can stay dispersed even in a crowded environment. Therefore, nonionic surfactants theoretically can be more beneficial for dispersing NPs in cementitious systems, where ionic strength and particle concentration are both very high.

Two important parameters are often used to characterize the surfactant molecules: critical micelle concentration (CMC) and hydrophilic-lipophilic balance (HLB) value. CMC indicates the concentration when surfactant molecules start to form micelle structures in solutions. HLB is based on the relative size and strength of the hydrophilic and hydrophobic parts of a surfactant. A high HLB value means the surfactant is more water-loving, while a low HLB value means the surfactant is more oil-loving.

3. Experimental work

In the present study, the raw materials (Portland cement and NS) were first characterized for their properties, and the results are shown in Table 1. Second, the optimal duration of ultrasonication was determined as it was then used for dispersing NS in various solutions. Third, 1% NS (by weight of the cementitious materials) was dispersed in aqueous solutions (called NS suspensions) and in cement pore solutions (called cement-NS suspensions) with different surfactants and ultrasonicated for the optimal duration. The cement pore solution was prepared by the centrifuge method, as described in Section 3.2.2. Then, all NS suspensions were evaluated for dispersion and stability using DLS and sedimentation tests as well as image analysis. Next, NS suspensions were prepared using surfactants that were the most effective in deagglomeration and stabilization of NS and were analyzed under TEM. TEM image and EDS analyses were then further performed to gain more quantitative information. Finally, the effects of selected surfactants on the flowability and early-age compressive strength of cement-NS paste were evaluated.

3.1. Materials

Materials used in this study were Portland cement, NS, seven different surfactants, and de-ionized water. Type I/II Portland cement, satisfying ASTM C150 [36] criteria, was used to prepare cement pore solution and cement paste. The cement had a specific gravity value of 3.14 and Blaine fineness of 376 m^2/kg. NS, supplied by Millipore Sigma Inc., Germany, had a particle size of 10–20 nm (BET), with 99.5% purity on trace metals analysis. The as-received powder NS showed quasi-spherical particles with micro-sized agglomerates under a scanning electron microscope (SEM) in secondary electron (SE) mode [32]. All properties of NS and Portland cement are presented in Table 1.

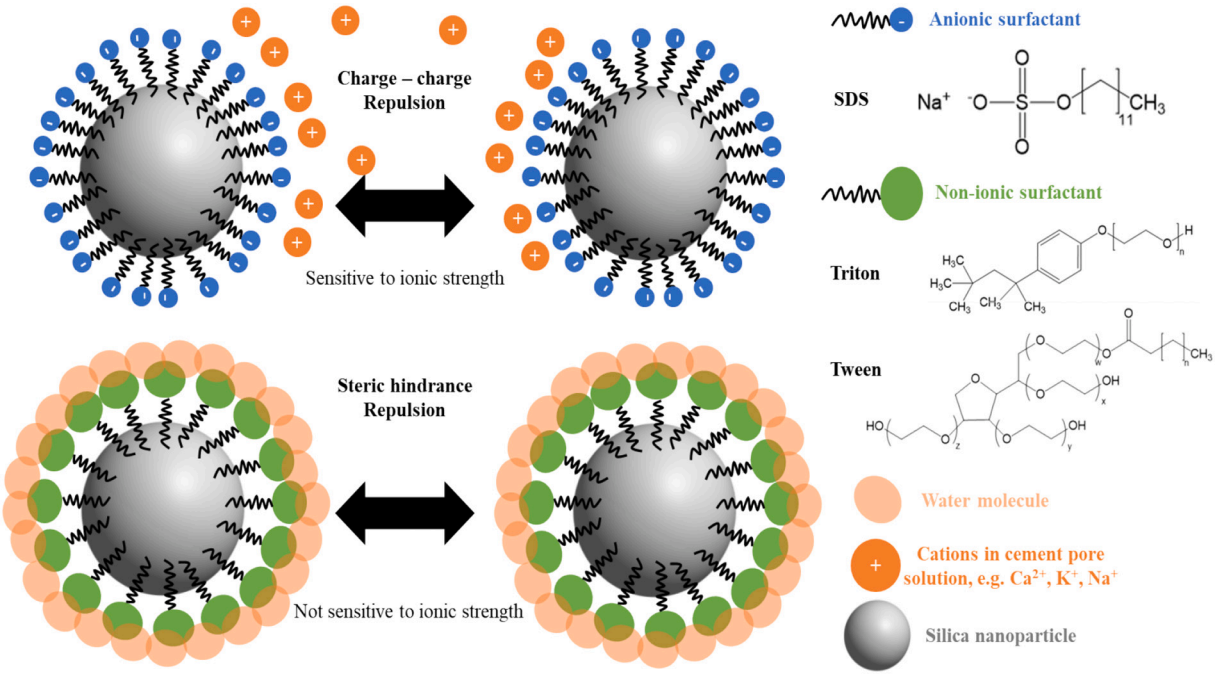

Fig. 1. Schematic showing stabilization of NS using surfactants.

Table 1
Properties of Portland cement and nanosilica.

Type I/II Portland cement		Nanosilica (NS)	
Oxide	%	Property	Value
SiO_2	20.05	Colour appearance	White
Al_2O_3	4.34	Form appearance	Dry powder
Fe_2O_3	3.05	Particle geometry	Quasi-spheres
CaO	63.18	Particle size (BET), nm	10–20
MgO	2.24	Molecular weight, g/mol	60.08
SO_3	3.18	Purity (trace metals analysis), %	99.5
Na_2O	0.09	Density (at 25 °C), g/mL	2.2–2.6
K_2O	0.68	Bulk density, g/mL	0.011
Others	0.85		
LOI	2.55		

The surfactants and their properties, such as the functional group, chemical formula, molar mass, hydrophilic-lipophilic values (HLB), and critical micelle concentration (CMC), are presented in Table 2. The chemical structure of these surfactants was shown in Fig. 1. PCE was used at 0.8% by weight of the cementitious materials (cement and NS), which was the highest dosage recommended by the manufacturer (BASF Chemicals Company). All other surfactants were used at 0.01% by weight of cementitious materials used in a paste with a water-to-binder ratio (w/b) of 0.45. The dosages of these surfactants were kept at 0.01% because a higher dosage might lead to form micelles due to their low CMC values.

3.2. Sample preparation

3.2.1. Ultrasonication and optimal duration

A probe sonicator (MISONIX Incorporated model XL2020) having an output frequency of 20 kHz and 600 W generating power was used for dispersing NS in aqueous and cement pore solutions. It should be noted that the ultrasonic waves can heat the specimen, which is undesirable. Two steps were taken to avoid the heating: (1) instead of the continuous mode, the sonicator was operated in a 5-second pulse on and 1.5-second pulse off mode; and (2) the vial containing the specimen was kept in an ice-water bath.

At first, the optimum time of sonication was determined by varying the time from 10 to 60 min and measuring the size distribution of NS in the aqueous solution using DLS. The intensity-weighted particle size distribution (PSD) is presented in Fig. 2(a). The calculated mean particle size (Z-average or Z-avg.) is plotted in Fig. 2(b). With the increase of sonication time, the shifting of the PSD curve towards the left in Fig. 2(a) suggested that the ultrasonication was quite effective in breaking up the agglomerates of NS. No substantial reduction in Z-avg. [Fig. 2(b)] was observed as the solution was sonicated for 10 min. However, as the time of sonication was increased from 10 to 20 min, Z-avg. reduced by approximately 76% (from 4363 ± 44 nm to 1020 ± 23 nm). A sonication time of 30 min furnished Z-avg. of 870 ± 13 nm. However, only minimal improvements in size reduction were obtained with a further increase in sonication time to 45 and 60 min. Therefore, considering the energy-saving and the experimental errors, 30 min was selected as the optimum ultrasonication time. All suspensions were then prepared at this

Table 2
Properties of surfactants used in this study.

Surfactant group	Name of the surfactant	Chemical formula	Avg. mol. wt. (g/mol)	HLB	CMC (mM)
Anionic	Polycarboxylate ether (PCE)	$CH_3(COO^-)_n$	~12,300	–	–
	Sodium dodecyl sulfate (SDS)	$CH_3(CH_2)_{11}OSO_3Na$	~288	40	–
Non-ionic	Tween 20 (T20)	$C_{58}H_{114}O_{26}$	~1228	16.7	0.059
	Tween 40 (T40)	$C_{62}H_{114}O_{26}$	~1277	15.6	0.027
	Triton X-114 (TX114)	$C_{14}H_{22}O(C_2H_4O)_{7-8}$	~537	12.4	0.200
	Triton X-100 (TX100)	$C_{14}H_{22}O(C_2H_4O)_{9-10}$	~647	13.5	0.230
	Triton X-405 (TX405)	$C_{14}H_{22}O(C_2H_4O)_{40}$	~1968	17.9	0.810

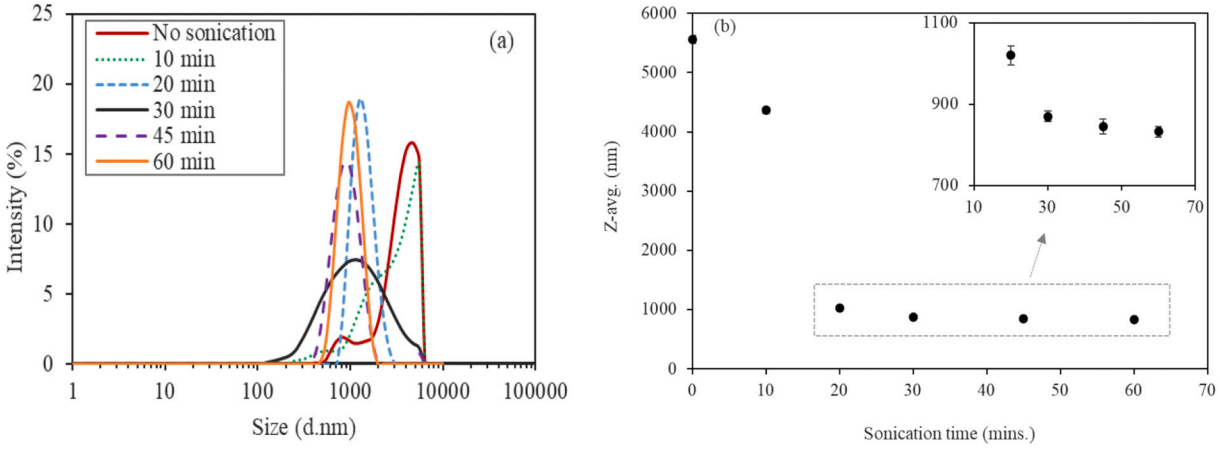

Fig. 2. PSD (a) and Z-avg. (b) of NS in aqueous solution with varying times of ultrasonication (inset in (b) shows the Z-avg. for 20 to 60 min of ultrasonication).

optimum time.

3.2.2. Preparation of cement pore solution

Cement pore solution was prepared by the centrifugation method. Firstly, a cement paste (without NS and surfactants) was prepared at a w/b of 0.45 using a Hobart mixer. The fresh cement paste was then transferred into 50 mL small vials, and the vials were kept in a Sorvall centrifuge. The centrifugation was then performed for 5 min at 5000 rpm, after which the solid and liquid parts were separated. The liquid was then collected and transferred to separate vials. The collected liquid was filtered three times with Whatman™ No. 2 filter papers to remove as many cement particles as possible. The filtered liquid was then kept in a clean vial and was used as the cement pore solution. Fig. 3 shows the cement paste before and after centrifugation. The pH value of the solution was measured to be 12.78, which represented a higher calcium concentration and higher alkalinity of the solution.

3.2.3. Preparation of NS and cement-NS suspension

1% NS (by weight of binder in a paste with a w/b of 0.45) was used throughout this study. To prepare NS suspension, 0.44 g of NS was first mixed with 20 mL of de-ionized water. A surfactant was then added, and the resulting solution was ultrasonicated for 30 min to obtain the NS suspension. The same sequence was followed to prepare cement-NS suspension, but the cement pore solution was used to replace de-ionized water. The prepared suspensions were then diluted for the DLS and TEM analyses. For example, 0.1 mL aliquot of NS, cement, and cement-NS suspension were further diluted into 1.1 mL of DI water and cement pore solution, respectively.

3.2.4. Preparation of cement-NS pastes

To prepare cement-NS paste, NS suspension, obtained from ultrasonication of NS and a selected surfactant in water, was used as "mixing water" to be added into cement. With a w/b of 0.45, the mixture was then mixed in a high-shear mixer for 2 min. The resulting cement-NS paste was then used to test for flowability and to cast six 2-inch cubic specimens for strength tests.

3.3. Tests and methods

3.3.1. Characterization of NS and cement-NS suspensions

3.3.1.1. Dynamic Light Scattering (DLS). DLS is the most commonly used method for determining the size distribution of NPs dispersed in a solution. It is based on elastic Rayleigh scattering and measures the velocity at which particles move under the Brownian motion by monitoring the intensity of light scattered by the sample [37]. The velocity of the Brownian motion is measured in terms of translational diffusion coefficient (D), which is then converted to the particle size using the Stokes-Einstein equation [Eq. (1)].

$$D_H = \frac{kT}{3\pi\eta D} \tag{1}$$

where 'D_H' is the hydrodynamic diameter, 'k' is the Boltzmann's constant, 'T' is the absolute temperature, 'η' is the viscosity, and 'D' is the diffusion coefficient. The hydrodynamic diameter, D_H, is the diameter of a hypothetical hard sphere that diffuses at the same rate as the particle being measured. In practice, though, particles in solution might be non-spherical, dynamic, and solvated. Therefore, D_H is indicative of only the apparent size of the dynamic hydrated/solvated particle. The diffusion

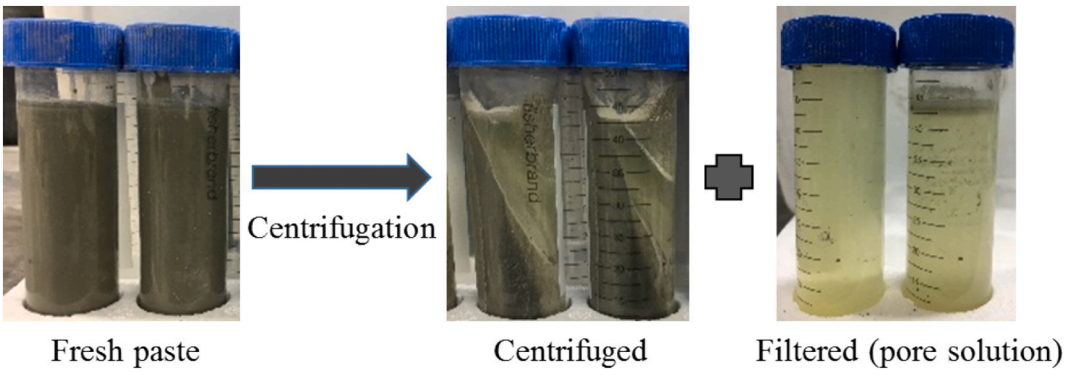

Fig. 3. Cement paste before and after centrifugation.

coefficient, *D*, is dependent on the size and surface structure of the particle and the concentration and type of ions in the medium [37]. Small-sized particles have a higher value of '*D*' and vice-versa. The first-order result from a DLS experiment is an autocorrelation function. The function is then analyzed to produce an intensity distribution of particle sizes. The intensity distribution is naturally weighted according to the scattering intensity of each particle fraction or family. The mean hydrodynamic diameter (Z-avg.) and polydispersity index (PDI) can also be calculated from the cumulants analysis. Z-avg. is a hydrodynamic parameter and is only applicable to particles in dispersion or molecules in a solution. A high Z-avg. generally indicates that the mean diameter of particles dispersed in a solution is high, while a high PDI suggests that the sample has a very broad size distribution.

DLS can also be utilized to measure the zeta potential (ZP) of NPs, which is the potential difference between the dispersion medium and the stationary layer of fluid attached to the dispersed particle. It is measured as the magnitude of the overall charge on the slipping plane of a particle dispersed in a solution. ZP is a key indicator of the stability of colloidal suspensions. For suspensions of small particles, a large ZP magnitude (often larger than ±25 mV [34]) usually suggests good stability or good resistance to aggregation.

A DLS-based instrument, Zetasizer Nano ZS (Malvern Instruments Ltd.), was used in this study for analyzing the PSD and ZP of NS dispersed in aqueous and cement pore solution. This instrument has an operating range of 0.3 nm to 10 μm. It releases a laser beam of 632 nm wavelength and collects signals with a backscattering configuration at an angle of 173 degrees. For the PSD and ZP analysis, a small specimen (approx. 5 μl) of aqueous/cement pore solution containing NS was taken and diluted with the corresponding continuous phase of the original specimen. The diluted specimen was then analyzed under Zetasizer. The intensity-weighted distribution of NS particles, Z-avg., PDI, and ZP were obtained as results.

3.3.1.2. Sedimentation. The stability of NS dispersion was also evaluated with the sedimentation test. The settlement rate of various NS suspensions was monitored visually as well as by capturing images with time. The images were captured at elapsed times of 0, 6, 12, 24, 48, 72, and 96 h. The distance between the vial containing the specimen and the camera was kept constant. The captured images were then analyzed using ImageJ software to extract quantitative information. It was assumed that as the aggregates of NS formed with time, these settled down under gravity and formed sedimentation at the bottom of the vial. Under this assumption, the sedimentation depths were calculated for the captured images using the software, as shown in Fig. 4. The depth of sedimentation, determined from this analysis, provides a quantitative measure of the performance of various surfactants.

3.3.1.3. TEM and image analysis. In transmission electron microscopy (TEM), a beam of electrons is transmitted through a sample to obtain an image on a fluorescent screen or a photographic film. Owing to a smaller wavelength of electrons used, TEM is capable of imaging at a much higher resolution. Features in a size range of 0.1 nm to 5 μm can be analyzed. In this study, FEI Tecnai F30 Electron Microscope (with <1.4 Å resolution) was used. It uses a LaB_6 electron gun that can apply up to 200 kV of accelerating voltage. Bright-field (BF) and dark-field (DF) images can be obtained with high-pixel resolution. In this study, samples of NS and cement-NS suspensions were analyzed under TEM. Tiny droplets of the diluted sample were deposited on a Formvar film that rested on a grid to prevent the charging of the sample. TEM-BF images were obtained at different magnifications and resolutions. For characterizing the various phases observed in the cement-NS suspension. EDS spot analysis was also performed.

Using ImageJ software, the analysis was further performed on these images to gain more quantitative information. The analysis procedure is shown in Fig. 5. The measurement scale was first calibrated. The image was then filtered using a bandpass filter that removed high spatial frequencies (blurring the image) and low spatial frequencies (subtracting the blurred image). The large structures in the image were filtered down to 20 pixels, and the small structures were filtered up to 2 pixels. Using thresholding, the features of the greyscale image were adjusted to segment NPs and agglomerates (features of interest) with the background. The particles in the threshold image were then measured and counted based on the defined parameters of size (zero to infinity) and circularity (0–1). An output image was also obtained with the aggregates of NPs shown in the form of ellipses and outlines (Fig. 5). A histogram of number PSD was then developed from the number counts of the particles in an image. Several images of a suspension were analyzed to obtain the number PSD of that particular suspension.

3.3.2. Tests for cement pastes

3.3.2.1. Flowability. The surfactants that exhibited good efficacy in dispersing NS were tested for their effects on the flowability and compressive strength of cement-NS paste. The flowability was measured using a mini-slump cone. This method is used to evaluate the consistency and early stiffening of the cement paste according to the modified ASTM C1611 standard [38]. It is merely a small version of the slump cone that is very commonly used for measuring the workability of a concrete mix. The cone has a bottom diameter of 40 mm, a top diameter of 20 mm, and a height of 54 mm. The diameter of the paste spread after lifting the cone is measured.

3.3.2.2. Early age strength. The tests for compressive strength of the paste were performed on a set of three 2-inch cubic specimens at curing

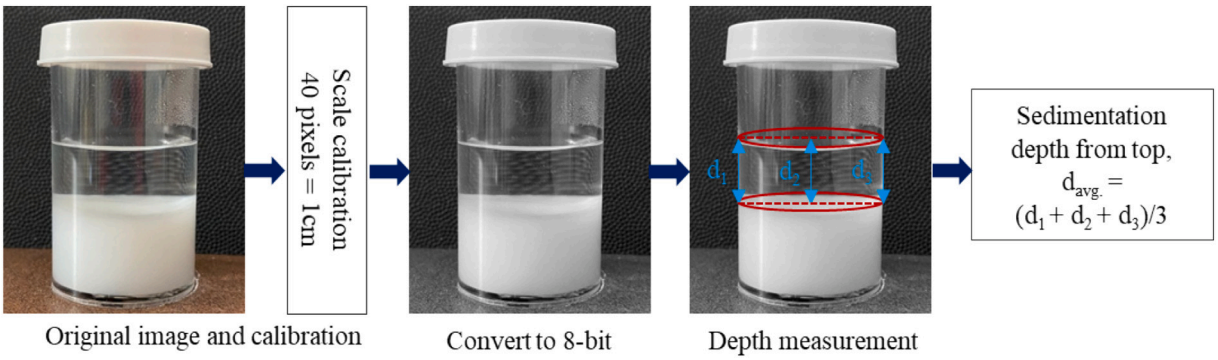

Fig. 4. Measuring sedimentation of NS with time.

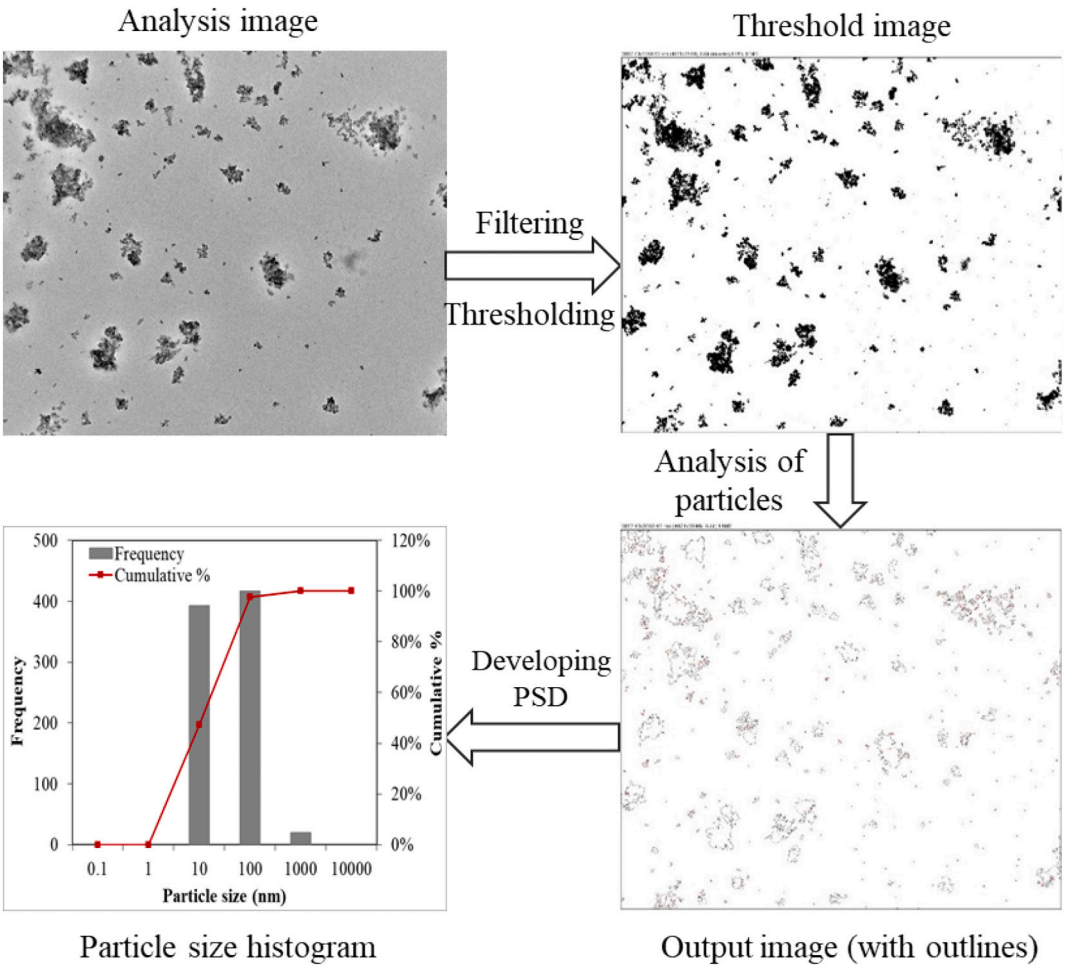

Fig. 5. Analysis of TEM images to obtain NS size distribution.

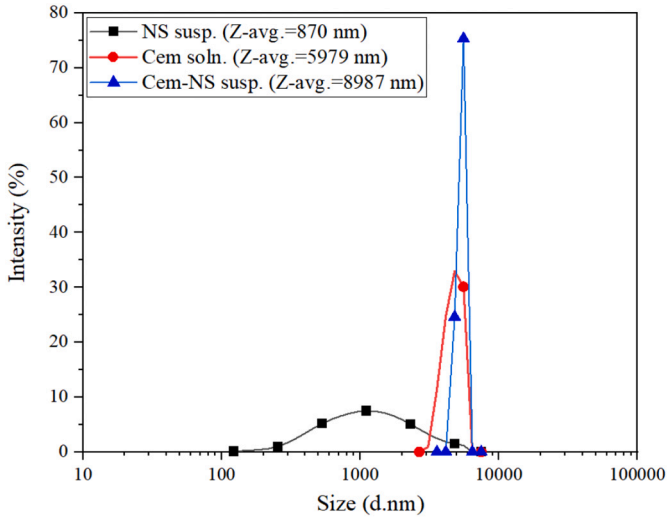

Fig. 6. PSD plots of control NS, cement, and cement-NS suspensions (without any surfactant).

ages of 1 day and 3 days. ASTM C109 [39] test procedure was followed.

4. Results and discussion

4.1. Effect of surfactants on dispersion

Fig. 6 shows the intensity-weighted PSD curves of NS dispersed in aqueous solution (NS suspension), cement pore solution, and NS dispersed in cement pore solution (cement-NS suspension) obtained from DLS tests. No surfactant was used for these suspensions. It can be seen that the PSD of NS suspension is very wide, whereas that of cement solution is narrow. This suggested that the centrifuged and filtered cement pore solution contains some fine cement particles with sizes ranging from 3 μm to 9 μm. The PSD of cement-NS suspension is the narrowest suggesting that some NS might have either agglomerated under the highly alkaline environment or adsorbed on the surfaces of cement particles, thus increasing the particle sizes in the cement-NS suspension. If a filter paper with smaller pores was used, the effect of cement particles on the DLS test results might have reduced. However, as discussed later in Section 4.4, having some unfiltered cement particles in cement-NS suspension helped observe the hydration/pozzolanic reaction of NS particles in TEM analysis.

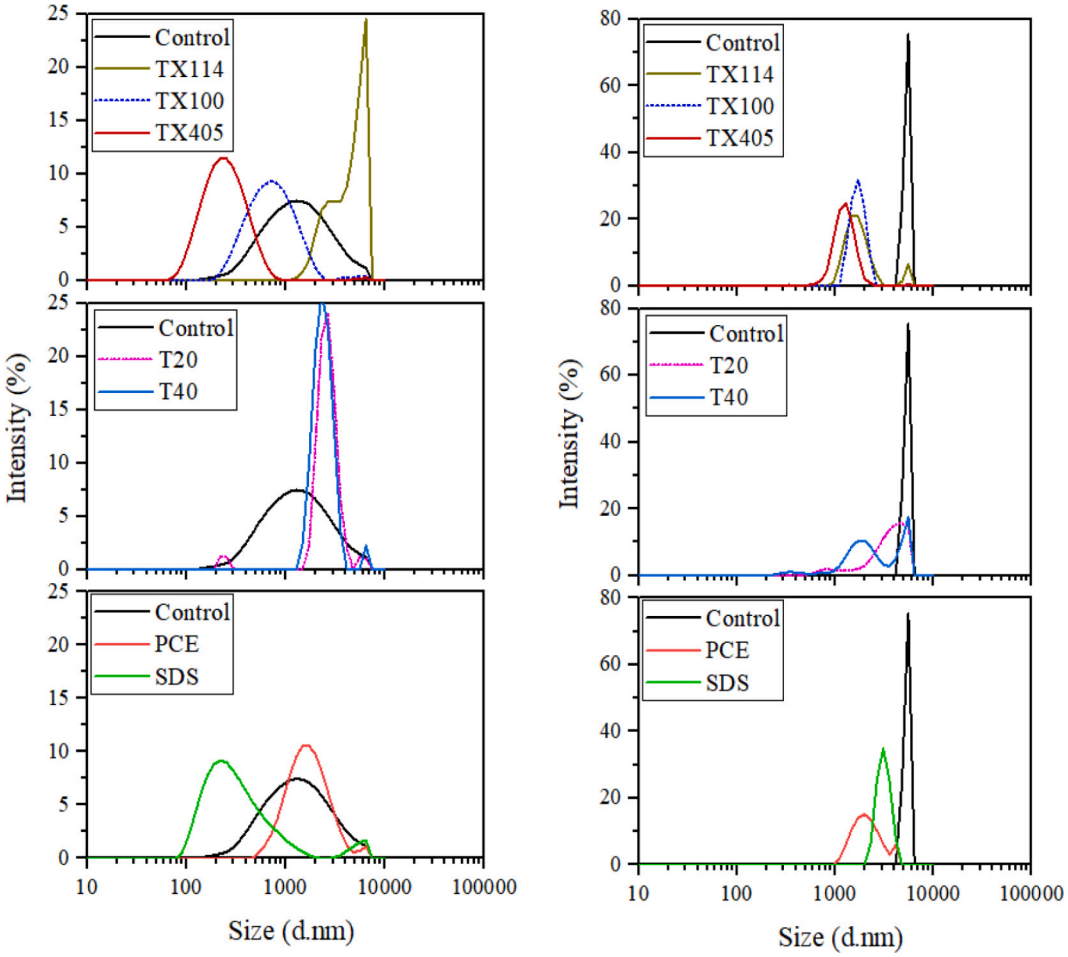

Fig. 7. PSD of NS dispersed with different surfactants in aqueous solution (a) and cement pore solution (b) [Control refers to the suspension with no surfactant].

4.1.1. Intensity-weighted PSD of NS suspensions

Fig. 7(a) shows the intensity-weighted PSD curves of NS suspension containing various surfactants. It can be seen from the figure that the particle size of the control suspension (no surfactant) ranged from approximately 200 nm to 8000 nm with a Z-avg. of about 900 nm, much larger than 10–20 nm (listed in Table 1), which indicates severe agglomeration. For suspensions with anionic surfactants, the particle size of the NS suspension containing 0.8% PCE ranged from 500 nm to 8000 nm with a Z-avg. slightly higher than 900 nm, not significantly different from that of control suspension. This suggests that the PCE surfactant was not effective for dispersion of NS in aqueous solution. Differently, the PSD curve of the NS suspension containing 0.01% SDS significantly shifted left, with particle size ranging from 70 nm to 2000 nm (Z-avg. around 240 nm), which is much lower than that of the control suspension. This indicates that SDS was much more effective than PCE surfactant for NS dispersion in aqueous solution.

For suspensions with nonionic surfactants, Fig. 7(a) illustrates that the Tween group behaved very differently from the Triton group. Compared with that of control NS suspension, the PSD curves of the two NS suspensions containing 0.01% Tween (T20 and T40) surfactants shifted to the right, with Z-avg. of around 3000 nm for both. Also, the PSD curves of these two suspensions exhibited a sharp and high peak, suggesting the presence of substantial NS agglomerates in the suspensions. Therefore, Tween surfactants were ineffective for NS dispersion.

Within the Triton nonionic surfactant group, Fig. 7(a) exhibits that NS suspensions containing 0.01% TX114 had more and larger agglomerates of NS than the control suspension as its PSD curve shifted to the right. Differently, PSD curves of suspensions containing 0.01% TX100 and TX405 shifted to the left, between which suspensions containing 0.01% TX405 was further left, suggesting that it was more effective for stabilizing NS dispersion. The particle size of the suspension containing 0.01% TX405 ranged from 60 nm to 600 nm with Z-avg. of 190 nm, the lowest among all suspensions studied. Thus, TX405 was the most effective surfactant for dispersing NS in aqueous solution among all surfactants studied.

4.1.2. Intensity-weighted PSD of cement-NS suspensions

Fig. 7(b) presents the intensity-weighted PSD curves of cement-NS suspensions containing various surfactants. As mentioned previously, the cement pore solution contains various ions, and it possesses high alkalinity and high ionic strength. The PSD curves of suspensions containing anionic surfactants PCE and SDS were observed on the left side of the control suspension, signifying a reduced particle size. The Z-avg. of cement-NS suspension with PCE was 2683 ± 260 nm, while that with SDS was 4160 ± 572 nm. This means that PCE was more effective than SDS in particle dispersion in the cement pore solution, which was different from that observed in NS suspensions.

The PSD curves of cement-NS suspensions containing two nonionic Tween group surfactants (T20 and T40) were also observed on the left side of the control suspension, signifying a reduced particle size. However, most particle sizes in these two suspensions were still larger than 1 μm. Two peaks are seen in the PSD curve of the suspension containing T40, revealing clusters of different sizes. The particle size of the suspension containing T20 ranged from 1 to 10 μm. Due to the presence of

separate peaks and the overlapping PSDs, the comparative efficacy of T20 and T40 in particle deagglomeration could not be established.

The efficacies of three nonionic Triton surfactants were relatively more discernible. PSD curves of cement-NS suspensions containing TX114, TX100, and TX405 were all on the left side of the PSD curve of control suspension. Once again, the PSD curve of suspension containing TX405 was further left, implying improved particle deagglomeration. The particle size of suspension containing TX405 ranged approximately from 500 nm to 2500 nm with a Z-avg. of 1640 ± 153 nm, even lower than the Z-avg. of suspension containing PCE (2683 ± 260 nm). Therefore, TX405 was also the most effective surfactant for dispersing NS in cement pore solution among all surfactants studied.

4.1.3. Comparisons of Z-avg. and PDI

To further understand the efficacy of various surfactants, Z-avg. and PDI of both NS and cement-NS suspensions were evaluated. Fig. 8(a) clearly shows that the Z-avg. values of cement-NS suspensions were all higher than those of corresponding NS suspensions containing various surfactants, except for TX114 surfactant. The following observations can be made from this figure: (1) for control suspension (no surfactant), the difference in Z-avg. values between the NS suspension and cement-NS suspension were large, but the difference is substantially reduced by the addition of surfactants. This indicates that these surfactants might have deagglomerated larger particles in cement pore solution; and (2) SDS (Z-avg. = 240 ± 2 nm) and TX405 (Z-avg. = 191 ± 2 nm) were the most effective surfactants for the dispersion of NS in aqueous solutions, while TX405 (Z-avg. = 1640 ± 153 nm) was the most effective surfactant for dispersion of particles in cement pore solution, followed by PCE surfactant (Z-avg. = 2683 ± 262 nm). This suggests that the TX405 surfactant could be used to prepare NS suspension and particle dispersion in cement-based materials, while PCE might be effective for cement particle dispersion but less effective for dispersion of NS in aqueous solution. The Tween group appeared to be ineffective in either NS or cement-NS suspensions.

Fig. 8(b) shows that compared with that of control suspension (no surfactant), PDI values of suspensions with surfactants were all lower. The PDI values of cement-NS suspensions were generally higher than those of NS suspensions, except that the differences in PDI between NS and cement-NS suspensions were very small for suspensions containing SDS and Triton group surfactants. It was minimal for suspensions with SDS and TX group. Among all surfactants studied, TX405 had the lowest PDI, 0.199 ± 0.013 for NS suspension, and 0.179 ± 0.066 for cement-NS suspension.

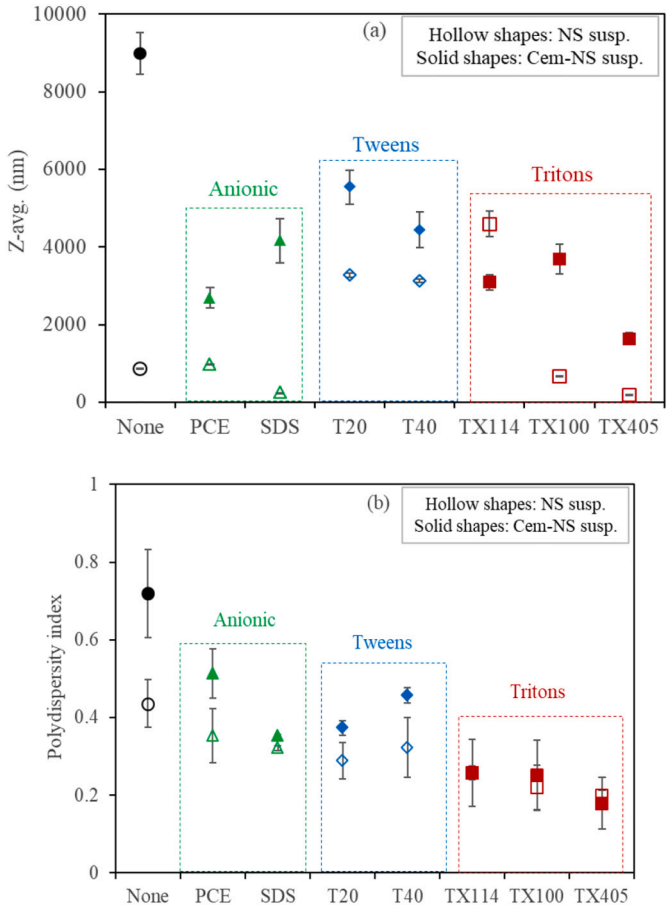

Fig. 8. Mean hydrodynamic size (Z-avg.) (a) and polydispersity index (PDI) (b) of NS and cement-NS suspensions made with various surfactants.

4.2. Effect of surfactants on stability

4.2.1. Zeta potential

Zeta potential (ZP) measurements of both NS suspensions and cement-NS suspensions containing various surfactants are presented in Fig. 9. The figure shows that all ZP measurements in the present study were negative values. The lower the ZP value (or the higher the absolute ZP value), it is the more likely that the suspension would have a better stability (From now on, ZP refers to its absolute value). For NS suspensions, Fig. 9 illustrates that the ZP value of suspension containing PCE was similar to that of control suspension (no surfactant), both of which were less than −10 mV, while ZP values of other suspensions, containing SDS, Tween and Triton group surfactants, were all higher, indicating improved stability. Among all NS suspensions, the ZP value of suspension containing TX405 was the highest (−24 ± 1.5 mV), followed by that of suspension containing SDS (−20 ± 1 mV).

For cement-NS suspensions, all ZP values were lower than those of corresponding NS suspensions. This implies that cement-NS suspensions were less stable than NS suspensions. Research has indicated that NS particles might be less stable in a high pH environment like cement solution [14]. There was no considerable difference in ZP values among control suspension and the suspensions containing PCE, SDS, T20, T40, and TX114 surfactants. Among all cement-NS suspensions, the ZP value of suspension containing TX405 was the highest (−18 ± 0.9 mV), followed by that of suspension containing TX100 (−11 ± 0.7 mV).

Based on the discussion above, it can be stated that the TX405 surfactant was effective in stabilizing particles in both NS and cement-NS suspensions.

4.2.2. Sedimentation

The captured images of sedimentation of NS in aqueous and cement

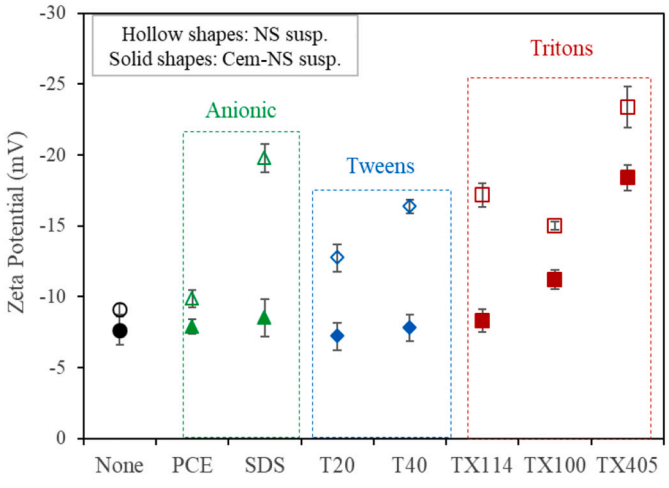

Fig. 9. Zeta potential of NS dispersed using various surfactants.

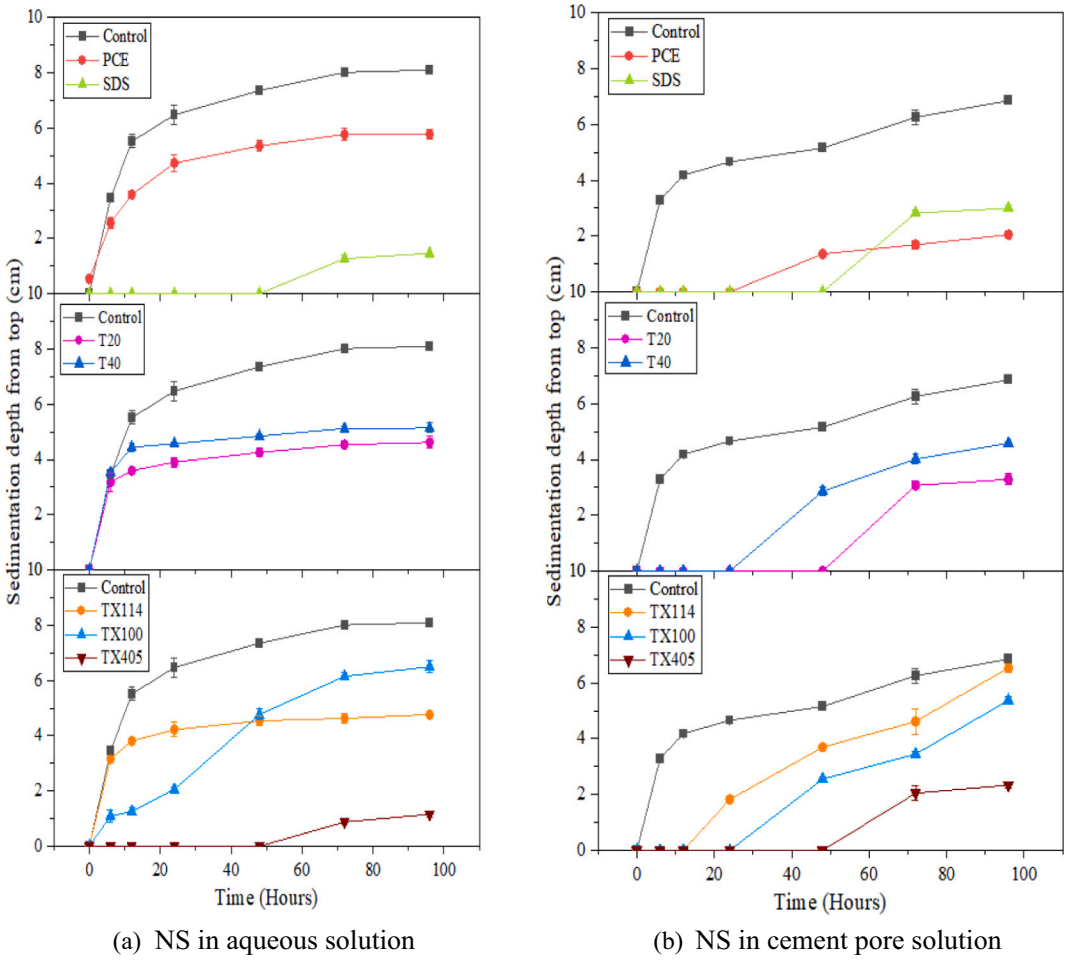

Fig. 10. Sedimentation depth of suspensions with various surfactants (a) NS suspension and (b) cement-NS suspension.

pore solution, dispersed using various surfactants, can be accessed from the Mendeley data [40]. Using image analysis, the depth of sedimentation (from top) with time was calculated, and the results are presented in Fig. 10. For NS suspensions, Fig. 10(a) shows that re-agglomeration and sedimentation of NS started at 6 h and continued thereafter in the control suspension (no surfactant). On the other hand, less sedimentation was seen in all suspensions containing surfactants. The sedimentation behavior of suspensions containing PCE, T20, T40, and TX114 surfactants was similar to that of control suspension, but the depths were smaller. The suspension containing the TX100 surfactant behaved differently. The sedimentation depth of this suspension increased much slowly with time but kept increasing until the end of the test (96 h). At 96 h, its sedimentation depth was next to that of control suspension (no surfactant), the highest among all suspensions with surfactants. Suspensions containing SDS and TX405 had the latest start of sedimentation and the lowest sedimentation depths among all suspensions studied.

For cement-NS suspensions, Fig. 10(b) shows that the control suspension (no surfactant) had the highest sedimentation depth among all suspensions studied, and it increased nonlinearly with time, which was similar to those in Fig. 10(a). Compared with Fig. 10(a), the magnitudes of sedimentation depths of all suspensions in Fig. 10(b) were smaller. This phenomenon might be related to the hydration of fine cement particles in the cement pore solution with time. The bulk volume of hydrated/hydrating cement particles is generally higher than that of unhydrated cement particles, thus reducing water volume in these samples. Another explanation of this phenomenon is the hydration of NS particles under the alkaline cement pore solution. Many research has confirmed that silica dissolves under an alkaline condition [41–43]. Due to the dissolution of silica ions, the electrokinetic potentials of the cement-NS suspensions were reduced, thus resulting in particle agglomeration, evidenced by their Z-avg. values. The agglomerates generally entrap pores and have a larger volume than their dispersed particles. Because of the increased volume of solids (cement grains and agglomerates) in the cement-NS suspensions, the sedimentation depths, measured from the clear water depths, of the cement-NS suspensions were consequently less than those of NS suspensions, which had a smaller Z-avg. In addition, the start time of many suspensions containing surfactants was delayed, and the latest was at 48 h for suspensions containing SDS, T20, and TX405 surfactants. At the end of tests (96 h), the lowest sedimentation depth occurred in the suspension containing PCE, followed by the suspension containing TX405 and then SDS surfactants. Comparing the difference in the sedimentation depths of NS suspensions and cement-NS suspensions without and with surfactants, one can infer that the PCE surfactant for stabilizing particles in the NS suspensions (Fig. 10(a)) appeared not as very effective as for stabilizing particles in cement-based suspensions (Fig. 10(b)), while the TX405 surfactant provided a superior stability for particles in both NS and cement-NS suspensions.

As mentioned previously, ZP measurements also reflect the stability of tested suspensions. Therefore, the relationship between ZP measurements and the sedimentation depths at 96 h of all suspensions was explored, and the result is presented in Fig. 11. A good correlation can be observed between these two parameters for NS suspensions (with aqueous solutions). The more negative value the ZP is, the less sedimentation of the suspension occurs. However, for the cement-NS suspensions, the relationship between ZP measurements and the

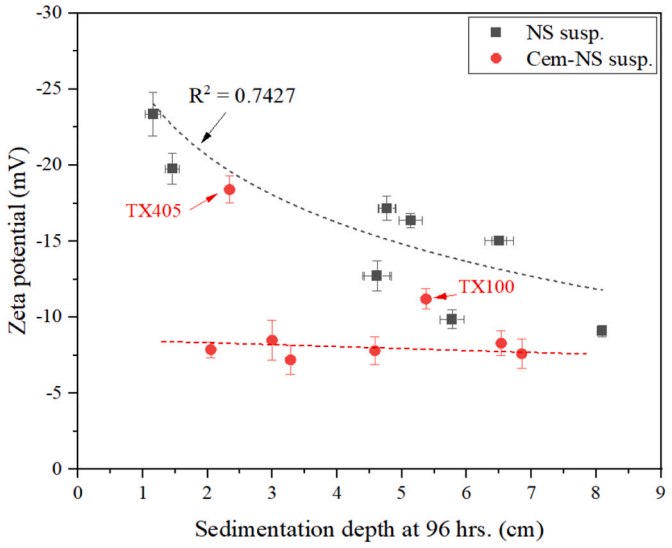

Fig. 11. Correlation of zeta potential and sedimentation depth.

sedimentation depths was not clear. (As discussed later, this might be partially attributed to the effect of cement hydration on sedimentation depths.) Most of these suspensions had a ZP value around 8–10 mV, but their sedimentation depths at 96 h ranged from 2 to 7 cm. There were two outliers: (1) the cement-NS suspension containing TX405 surfactant, which had a ZP value of −18 ± 0.9 mV and the 96-hour sedimentation depth of 2.4 ± 0.12 cm, and (2) the cement-NS suspension containing TX100 surfactant, which had a ZP value of −11 ± 0.67 mV and the 96-hour sedimentation depth of 5.37 ± 0.12 cm. This observation confirms the effectiveness of the TX405 surfactant in the stabilization of particles in cement-NS suspension.

4.3. Effect of surfactants on properties of cement pastes

From the analyses of particle size, ZP, and sedimentation, TX405 was proved to be the most effective surfactant in the deagglomeration and stabilization of NS. Therefore, further studies were performed using TX405 and were compared with the control (without any surfactant). The results are presented in this section.

4.3.1. Flowability

To evaluate the effect of TX405 on the flowability of cement paste, the mini-slump flow diameter of paste without NS was first measured. Besides, the flowability of two cement pastes – control and with PCE, was also tested. Fig. 12(a) presents a bar chart containing the mean flow diameter of the three pastes (mean of three specimens). The mean flow diameter of the control paste was 8.5 cm, while that in the case of TX405 (added at 0.01% by weight of cement) was 7.8 cm, which meant that the flow was reduced. On the other hand, the addition of PCE (at 0.4% by weight of cement) significantly improved the flow to 11 cm. The improvement in the flow due to PCE is usually interpreted by the dispersion mechanism of superplasticizers that explains the occurrence of more disassembled flocculated structure and a higher amount of entrapped water release in the presence of a superplasticizer [44,45].

Next, the effect of TX405 on the flowability of cement-NS paste was evaluated, as shown in Fig. 12(b). A very high surface area to volume ratio of NS increased the water demand. Therefore, the flow diameter of the control cement-NS paste (7.25 cm) was lower than that of the corresponding cement paste (8.5 cm). TX405 further reduced the flow diameter to 5.5 cm, whereas PCE increased the diameter to 11 cm. However, the dosage of PCE had to be increased, in this case, to 0.8% of the weight of cementitious materials that was twice the dosage used in cement paste without NS. Since a sufficient flow of cement-NS paste was not achieved using TX405 only, the casting of specimens for strength tests was difficult. Therefore, it was decided to use TX405 in combination with PCE to achieve sufficient flowability. It can be observed that this combination (0.8% PCE + 0.01% TX405) produced a flow diameter greater than 10.5 cm [Fig. 12(b)] that was adequate to cast specimens.

4.3.2. Compressive strength

The 2-inch cubic cement-NS paste specimens were tested for compressive strength at curing ages of 1 day and 3 day, as shown in Fig. 13. No significant improvement in the compressive strength was observed upon the addition of PCE. However, PCE + TX405 improved strength considerably. The compressive strength, in this case, was 18.5 MPa and 38 MPa, respectively, at 1-day and 3-days, which were approximately 33% and 41% higher than the corresponding strength values of the control paste. The improvement in strength can be attributed to- (1) the efficacy of TX405 in reducing the agglomerate size of NS, as evidenced by the DLS results; and (2) possible enhanced nucleation of CSH fibrils on NS surfaces owing to a better dispersion of NS achieved by TX405, as observed later in electron microscopy images.

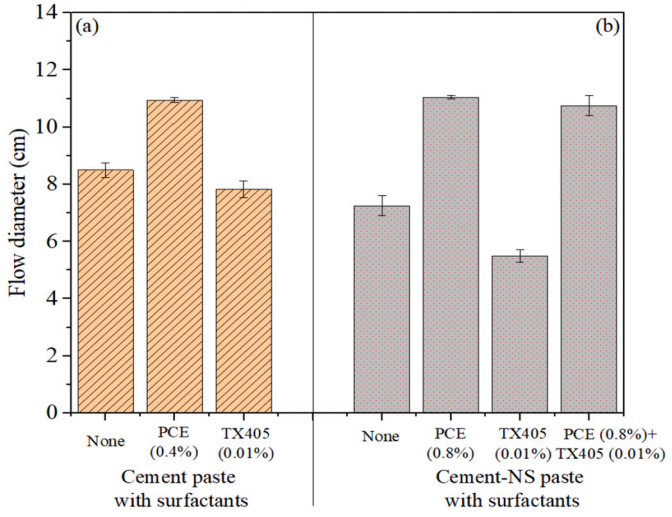

Fig. 12. Effect of surfactants on the flowability of cement pastes; (a) no NS and (b) 1% NS.

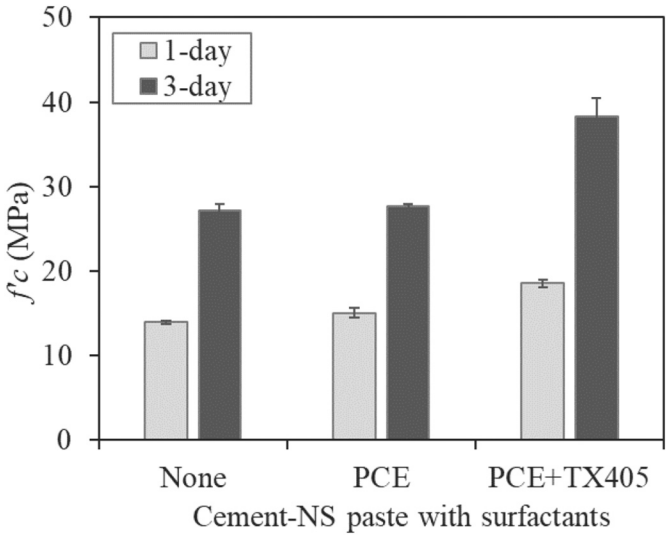

Fig. 13. Effect of surfactants on compressive strength of cement-NS paste.

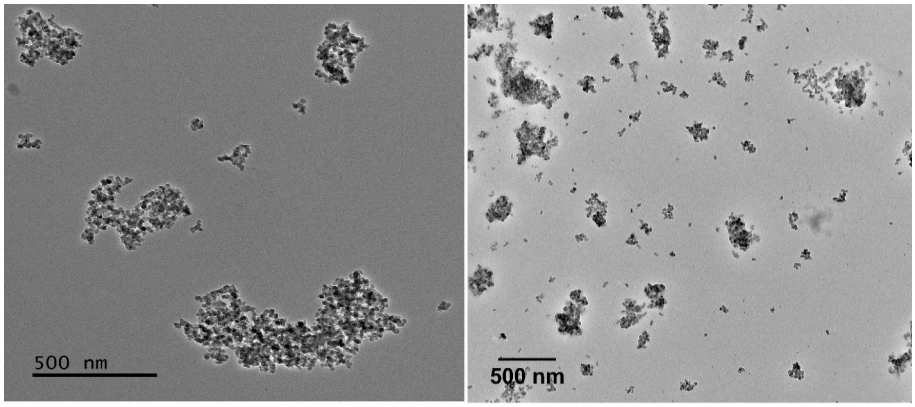

(a) NS suspension-Control (b) NS suspension-TX405

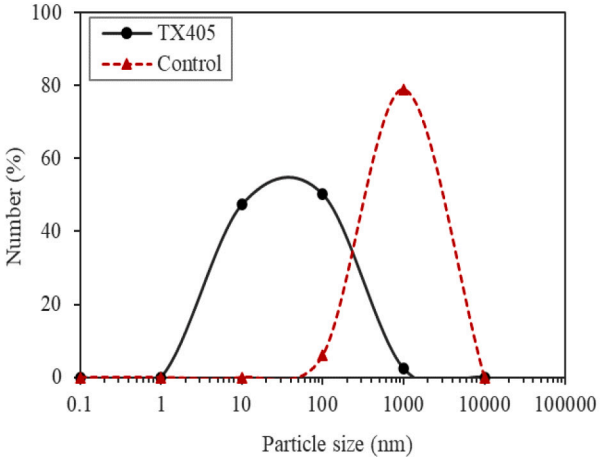

(c) Number PSD

Fig. 14. PSD of cement-NS suspension with no and TX405 surfactant from image analysis (a)–(b) TEM images; (c) PSD of the suspensions.

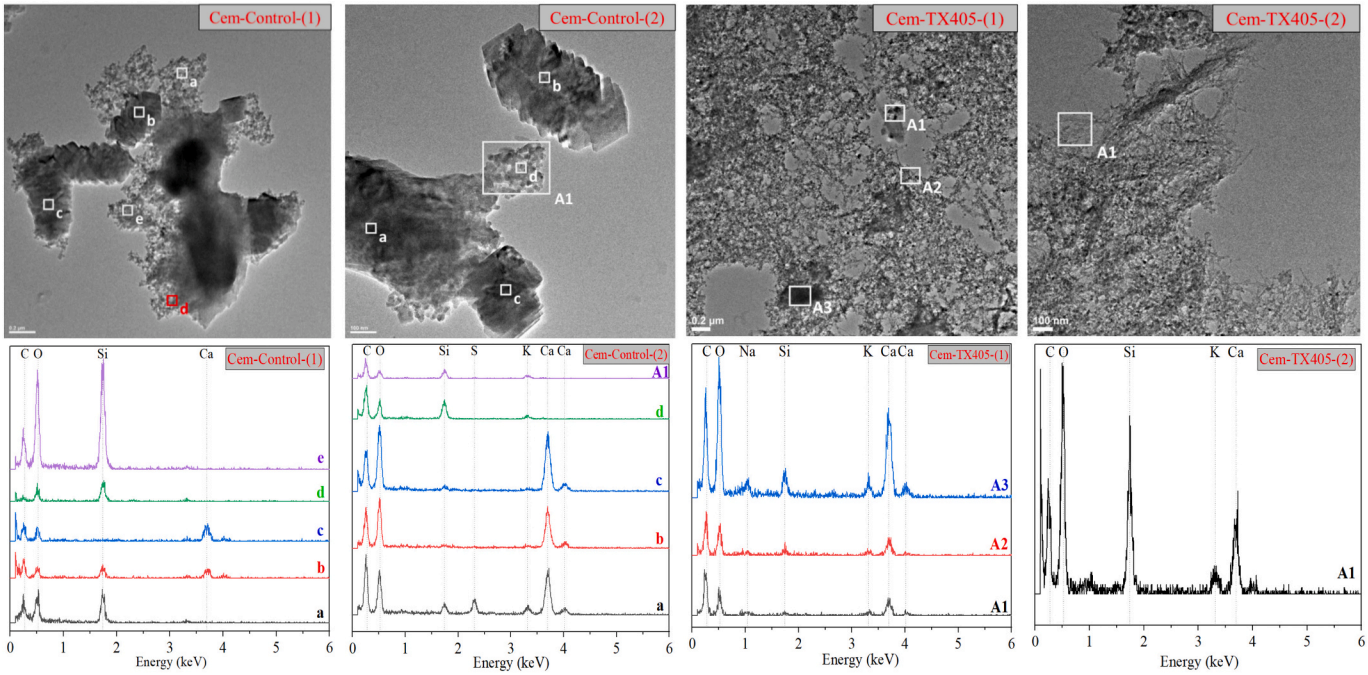

Fig. 15. TEM images (top) and EDS spectra (bottom) of control and TX405 cement-NS suspension (at 3 h).

4.4. TEM and image analysis

4.4.1. NS suspension

TEM images of control and TX405 NS suspensions are shown in Fig. 14. In the field of view of control suspension [Fig. 14(a)], most of the NPs could be seen to form clusters and agglomerates of size greater than 500 nm, with some even greater than 1 μm. Only a few smaller agglomerates could be observed in this case. On the other hand, NS in TX405 suspension [Fig. 14(b)] did not agglomerate heavily, with more than 80% of particles observed to be of a size less than 200 nm. TEM images were analyzed using ImageJ software to obtain quantitative information about the PSD (Fig. 5). A total of 828 and 1045 particles were analyzed for the control and TX405 suspension, respectively. The comparison of the number PSDs of control and TX405 suspensions is shown in Fig. 14(c). More than 50% of particles in control suspension were larger than 500 nm, whereas 80% of particles in TX405 suspension were smaller than 200 nm. The authors would like to point out that the PSD developed from TEM images should not be compared directly with that obtained from DLS since the former is the size distribution by number, whereas the latter is an intensity distribution. However, qualitatively both PSDs reveal that TX405 was able to effectively deagglomerate NPs in the aqueous solution.

4.4.2. Cement-NS suspension

TEM images of control and TX405 cement-NS suspensions are shown in Fig. 15. Various shapes with different darkness and morphology were observed in the images. To confirm they are different phases, spot EDS analysis was performed. The spots for EDS analysis were chosen based on the difference in morphology and darkness level of the observed phases so that the intermixing could be avoided, and the results depict the elemental composition of pure phases as accurately as possible. Along with the images, EDS spectra are also presented in Fig. 15. From the TEM images of control cement-NS suspension and their respective EDS spectra, three distinct phases with different morphology were observed:

(1) Irregularly shaped dark black spots - they predominantly consisted of calcium, silica, sulfur, and potassium (EDS spectrum of spot 'a' from "*Cem-control-(2)*" image). The morphology and elemental composition of these spots suggested that these were unhydrated cement particles (C_3S and C_2S) resulting from the cement pore solution.
(2) Light grey rounded particles and their clusters - their EDS spectra (spots 'a', 'd', and 'e' from "*Cem-control-(1)*" image and spot 'd' and area 'A1' from "*Cem-control-(2)*" image) suggested the presence of silicon without any trace of calcium. Therefore, it can be inferred that they were particles and clusters of NS. The presence of NS clusters reiterated that the particles of NS agglomerated heavily in the alkaline environment of cement pore solution as no surfactant was used to disperse them.
(3) Light black rectangular and stacked crystals – the average size of these crystals was around 100 nm. The EDS spectra (spot 'c' from "*Cem-control-(1)*" and spots 'b' and 'c' from "*Cem-control-(2)*" images) showed that these primarily contained calcium with very small or no traces of silicon, sulfur, aluminum, and potassium. Based on the elemental composition, the crystals could be either portlandite or calcite.

From the images of TX405 cement-NS suspension and their respective EDS spectra (Fig. 15), all three distinct phases that were observed in control suspension (no TX405) were observed in this case too:

(1) The presence of irregularly shaped dark black spots, or unhydrated cement particles (C_3S and C_2S), can be confirmed from the EDS spectrum of area 'A3' from the "*Cem-TX405-(1)*" image.

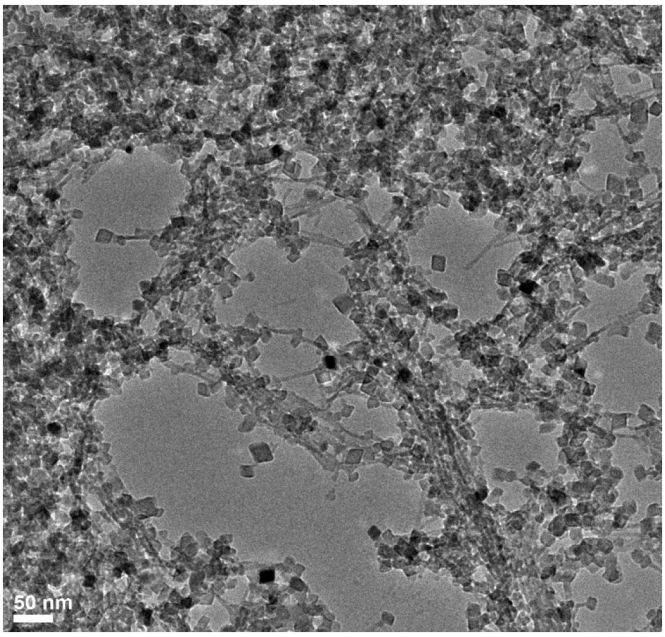

Fig. 16. TEM image of TX405 cement-NS suspension (at 3 h) showing the intermingling of rhombohedral calcite crystals and CSH fibers.

(2) The light grey rounded particles of NS were not clearly seen in images "*Cem-TX405-(1)*" and "*Cem-TX405-(2)*" but became visible in the image at higher magnification (Fig. 16).
(3) Light to dark rectangular crystals, containing primarily calcium, were shown by the EDS spectrum of area 'A1' in the "*Cem-TX405-(1)*" image. Those appeared rhombohedral crystals with a size around 10–20 nm, indicating that they were probably calcite.

In addition, a substantial amount of needle or fiber-like dendrites, of lengths on the nanometer scale, were observed in both the images of TX405 cement-NS suspension. The EDS spectra of these fibrous dendrites (area 'A2' from "*Cem-TX405-(1)*" and area 'A1' from "*Cem-TX405-(2)*" image) revealed that these primarily contained calcium and silicon with very small intensity peaks of sodium and potassium and no trace of aluminum and sulfur. The absence of aluminum and sulfur pointed that these fibers were not those of ettringite; instead, these were probably outer product (OP) CSH gel fibers. The fibril morphology of OP CSH gel resembled those found by previous studies in TEM analysis [46–49]. The OP CSH fibers generally nucleate on the surface of C_3S grains. In the cementitious system, NS could act as a seeding material and provide additional sites for the nucleation of OP CSH, called the "seeding effect" [48]. The precipitation and morphology of OP CSH nuclei formed on C_3S grains and seed material, however, are different. In the study on limestone as a seed in a C_3S paste, Bazzoni [47] observed that CSH preferentially precipitated on limestone surfaces. Also, OP CSH nuclei formed on limestone grains were well-oriented, needle or fiber-shaped, and perpendicular to grains' surface. In contrast, those formed on C_3S grains showed a divergent sea anemone morphology. Therefore, high precipitation of the needle or fiber-shaped products, observed in Figs. 15–16, was confirmed to be OP CSH nuclei. The composition of CSH is generally expressed by the atomic ratio of calcium to silicon (C/S). A wide range of C/S values has been measured, with most falling in the range of 0.7 to 2.3 [49]. Based on the EDS spot analysis, C/S of OP CSH analyzed in this study was in the lower range (0.6–0.7), which suggested that the atomic structure of CSH was tobermorite-like wherein part of the bridging tetrahedra were eliminated, and part of the protons were substituted with calcium ions [49]. A lower C/S of OP CSH could be due to (1) removal of calcium from CSH or (2) high loss of calcium during EDS analysis since the hydration products are highly prone to beam damage

[50].

Another important point of notice from Fig. 16 is the distribution of nanosized rhombohedral crystals in the matrix. These appear to be intermingled with the fibrillar structure of OP CSH gel and also seem distributed throughout the matrix. A similar distribution of crystals and gel in a Portland paste was observed by Richardson et al. [51], which were confirmed to be calcite. Calcite might have formed by the removal of calcium from CSH, which reduced C/S; however, the presence of calcite nanocrystals throughout the matrix led to the densification of the regions of OP CSH (Fig. 16). A densified CSH consequently improved the compressive strength of the paste, as presented earlier in Section 4.3.2.

From the visual examination of TEM images, a clear and direct qualitative distinction of the agglomeration behavior of NS particles in the two suspensions (control and TX405) could not be established. A quantitative distinction (using image analysis) was also difficult, unlike that in the case of the aqueous solution. However, clusters of NS particles were apparent in control suspension (Fig. 15), while these were not observed in TX405 suspension (Fig. 16). Besides, EDS analysis confirmed the nucleation of fibrous OP CSH gel in TX405 suspension, which was not present in the control suspension. According to the classical nucleation theory, the rate of heterogeneous nucleation (R) is directly proportional to the number of nucleation sites (N_s) [52]. The formation of a large number of fibril OP CSH nuclei in TX405 suspension suggested that a large number of nucleation sites were available in this system. This, in turn, meant that NS treated with TX405 in cement pore solution were better dispersed than those in the control suspension, which was consistent with the DLS results.

4.5. Further discussion

This section provides additional explanations for the roles of various surfactants in particle dispersion and stabilization of NS and cement-NS suspension, as well as their effects on paste flowability and early age strength. Based on the information presented in Sections 4.1–4.4, SDS and TX405 were the two most effective surfactants for the dispersion of NS in aqueous solution, while only TX405 was an effective surfactant for the dispersion of particles in the cement pore solution. Tween group surfactants did not yield promising results in the dispersion and stabilization of either NS or cement-NS suspension.

Between the two anionic surfactants used, the SDS surfactant performed better in NS suspension, while PCE surfactant performed better in cement-NS suspension. Generally, PCE superplasticizers are comb polymers consisting of an anionic backbone with carboxylic acid groups (COO^-) and grafted side chains, which mainly consists of hydrophilic polyethylene glycol (PEG) units [12]. SDS is the sodium salt of dodecyl hydrogen sulfate, the ester of dodecyl alcohol and sulfuric acid. It consists of a 12-carbon tail attached to a sulfate group. The hydrocarbon tail provides it the amphiphilic properties and superior surface adsorption characteristics. As discussed before, anionic surfactant stabilizes particles via the charging of the particles' surface. Fig. 9 shows a higher ZP value of NS suspension containing SDS. This was possibly because of the higher charge provided by SDS to the surfaces of NS that resulted in stronger long-range electrostatic repulsion, which prevented NS from agglomeration and led to smaller Z-avg. (Fig. 8). Consequently, the NS suspension containing SDS slowed the sedimentation process, as was observed in Fig. 10(a). However, the dispersion efficacy of SDS was drastically reduced in the highly alkaline (pH = 12.78) cement pore solution, which also consisted of counterions such as Ca^{2+} and K^+ cations. The counterions can effectively screen the electrostatic repulsion. Thus, SDS could no longer stabilize NS or fine cement particles in the system. As shown in Fig. 9, the ZP of NS dispersed with SDS in cement solution drastically dropped compared to that in water. In addition, Ca^{2+} may form bridges with anions on particle surfaces, leading to the formation of large particle agglomerates. Similar aggregates could also develop in a cement-NS suspension containing PCE [14]. However, PCE had a very high molecular mass (~12,300 g/mol) compared to that of SDS (~288 g/mol). Regardless of their molecular nature, molecular weight plays an important role in the adsorption of anionic surfactants [53,54]. With high molecular weight, PCE chains could adsorb strongly at the solid-liquid interface, thereby improving the repulsion between NS particles [55].

Between the two nonionic surfactant groups used, Tween surfactants are formed by the ethoxylation of the fatty acid esters of sorbitan. The different surfactants in this series can be differentiated by the number of repeat units of polyethylene glycol (PEG) after the ethoxylation process. For example, Tween 20 has 20 repeat units of PEG, and similarly, Tween 40 has 40 repeat units. On the other hand, Triton surfactants are prepared by the reaction of octylphenol with PEG. This group's surfactants are primarily differentiated based on the average number of PEG units in the ether side chain and the HLB values. TX114, TX100, and TX405 used in this study had 7–8, 9–10, and 40 PEG units, and their HLB values were 12.4, 13.5, and 17.9 (Table 2), respectively. Triton surfactants are generally considered more versatile emulsifiers than ionic surfactants because of their lack of reactivity and insensitivity to ions. Particle stabilization with nonionic surfactants is based on the steric repulsion forces from the hydration layers, which is not affected by the presence of counterions in the cement pore solutions. Therefore, nonionic surfactants of the Triton X series (TX) showed better dispersion performance with an increase of HLB value (Figs. 8–9). TX 405 with a higher HLB value of 17.9 enhanced dispersion stability and particle size distribution compared to control, TX 100, and TX114. Among the three Triton surfactants, the greatest efficacy of TX405 can be attributed to its high number of PEG units (40) and high HLB value. The presence of a high number of PEG units significantly improved the adsorption capability of TX405 at the solid-liquid interface and, consequently, steric repulsion between NPs [18,22]. Greater stability of suspensions was achieved due to a high HLB value.

The effect of nonionic surfactants can also be explained by their CMC values. CMC was observed to be highly correlated ($R^2 > 0.8$) with Z-avg. and PDI of cement-NS suspension and with the compressive strength of cement-NS paste [Fig. 17(a)–(c)]. Also, the compressive strength could be seen to decrease with an increase in Z-avg. and PDI [Fig. 17(d)–(e)]. In general, CMC is the concentration at which further addition of solute molecules might result in the formation of micelles while leaving the monomer concentration more or less unchanged at the CMC [35]. T20 and T40 have lower CMC than Triton surfactants (Table 2). The adsorption of surfactant molecules on the NP surface will be affected by the micelle formation through the dynamical exchange of surfactants. For example, at the same concentration (0.01% by weight), Tween surfactants (CMC 0.02–0.06 mM) would form more micelles and have less 'free' surfactant molecules to adsorb onto the particles than those in the case of Tritons (CMC 0.2–0.8 mM). In this system, it may be more energetically favorable for the surfactant molecules to stay in a micelle assembly than adsorbing onto a hydrophilic surface of the NS particle. At the same time, the CMC values for Triton surfactants are a magnitude higher than those of Tweens. This means that Triton surfactants would have freer surfactant molecules to adsorb onto the surface of the particles and stabilize them. Moreover, the correlation in the Triton series was consistent with the proposed mechanism. As CMC value increased from TX114 to TX405, so did the compressive strength of cement-NS paste.

5. Conclusions

The efficacy of two anionic and five nonionic surfactants in dispersing dry powder NS (10–20 nm) was analyzed in this experimental study. The effective surfactants were selected based on the results from DLS and sedimentation tests and analyzed for their effects on the early-age properties of the cement-NS paste. Specific conclusions from this study are as follows:

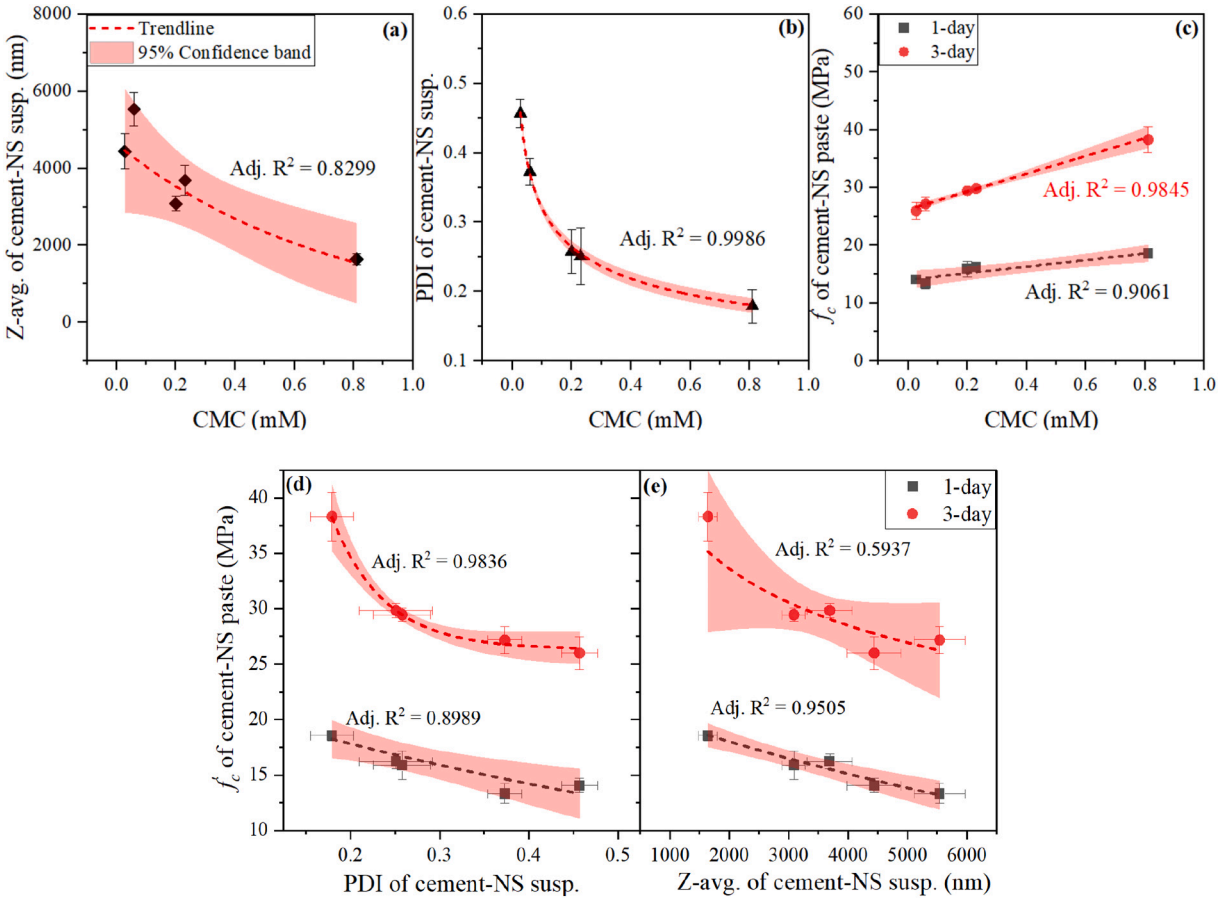

Fig. 17. Correlation between the parameters of DLS and cement-NS paste and CMC of nonionic surfactants.

(1) DLS test results show that without surfactant, the particle size of the NS suspension, after 30 min. of ultrasonication, ranged from approximately 200 nm to 8000 nm with a Z-avg. value around 900 nm, indicating a severe agglomeration. Although showing different effectiveness, all surfactants deagglomerated particles in cement-NS suspensions; however, not all surfactants deagglomerated particles in NS suspensions. Surfactants T20, T40, and TX114 aggravated NS agglomeration in aqueous solution.

(2) DLS and sedimentation test results show that among all surfactants studied, TX405 was the most effective surfactant for deagglomeration and stabilization of NS in aqueous solution, followed by SDS. TX405 was also the most effective surfactant for deagglomeration and stabilization of particles in cement-NS suspensions, followed by PCE.

(3) A good correlation between the zeta potential (ZP) and the 96-hour sedimentation depth of NS suspensions was observed. Generally, the higher the magnitude of ZP, the smaller sedimentation depth the NS suspension has. However, this trend was not observed in cement-NS suspensions, possibly due to the effect of cement hydration on the measurement of sedimentation depth.

(4) The addition of 1% NS and 0.01% TX405 decreased the flowability of cement paste, while the addition of 0.8% PCE surfactant significantly increased the flowability of the cement paste. Adequate flowability of the cement-NS paste was achieved when 0.01% TX405 and 0.8% PCE were used together.

(5) The cement-NS paste with 0.01% TX405 and 0.08% PCE exhibited a 33% and 41% increase in compressive strength at 1-day and 3-days, respectively, compared to the cement-NS paste (with no surfactant). TEM and EDS analyses indicate that enhanced nucleation of outer product CSH gel and densification of its regions due to the formation of calcite nanocrystals were probably responsible for the strength improvement.

(6) The Z-avg. and PDI values of cement-NS suspensions and the compressive strength of cement-NS pastes exhibited highly correlated relationships with the CMC of nonionic surfactants, suggesting that the improved particle dispersion was another reason for the paste strength improvement.

CRediT authorship contribution statement

Yogiraj Sargam: Conceptualization, Methodology, Investigation, Formal analysis, Data curation, Writing- Original Draft; **Kejin Wang**: Conceptualization, Methodology, Resources, Supervision, Funding acquisition, Writing- Review and Editing; **Ayuna Tsyrenova**: Conceptualization, Investigation, Writing- Review and Editing; **Shan Jiang**: Conceptualization, Methodology, Resources, Supervision, Funding acquisition, Writing- Review and Editing; **Fei Liu**: Investigation, Formal analysis.

Declaration of competing interest

The authors declare that they have no known competing financial interests or personal relationships that could have appeared to influence the work reported in this paper.

Acknowledgments

This is a part of the first author's Ph.D. dissertation, and he would like to acknowledge the support of the Department of Civil, Construction, and Environmental Engineering at Iowa State University (ISU) for

his Ph.D. study. The support provided by Steve Veysey (Chemical Instrumentation Facility, ISU) for the DLS test is also gratefully acknowledged.

References

[1] F. Sanchez, K. Sobolev, Nanotechnology in concrete - a review, Constr. Build. Mater. 24 (2010) 2060–2071, https://doi.org/10.1016/j.conbuildmat.2010.03.014.

[2] G. Bastos, F. Patiño-Barbeito, F. Patiño-Cambeiro, J. Armesto, Nano-inclusions applied in cement-matrix composites: a review, Materials (Basel). 9 (2016) 1–30, https://doi.org/10.3390/ma9121015.

[3] M. Gesoglu, E. Güneyisi, D.S. Asaad, G.F. Muhyaddin, Properties of low binder ultra-high performance cementitious composites: comparison of nanosilica and microsilica, Constr. Build. Mater. 102 (2016) 706–713, https://doi.org/10.1016/j.conbuildmat.2015.11.020.

[4] E. Ghafari, H. Costa, E. Júlio, A. Portugal, L. Durães, The effect of nanosilica addition on flowability, strength and transport properties of ultra high performance concrete, Mater. Des. 59 (2014) 1–9, https://doi.org/10.1016/j.matdes.2014.02.051.

[5] B.-W. Jo, C.-H. Kim, G. Tae, J.-B. Park, Characteristics of cement mortar with nano-SiO2 particles, Constr. Build. Mater. 21 (2007) 1351–1355, https://doi.org/10.1016/j.conbuildmat.2005.12.020.

[6] A. Nazari, S. Riahi, The effects of SiO2 nanoparticles on physical and mechanical properties of high strength compacting concrete, Compos. Part B Eng. 42 (2011) 570–578, https://doi.org/10.1016/j.compositesb.2010.09.025.

[7] Z. Rong, W. Sun, H. Xiao, G. Jiang, Effects of nano-SiO2 particles on the mechanical and microstructural properties of ultra-high performance cementitious composites, Cem. Concr. Compos. 56 (2015) 25–31, https://doi.org/10.1016/j.cemconcomp.2014.11.001.

[8] L. Senff, D. Hotza, W.L. Repette, V.M. Ferreira, J.A. Labrincha, Mortars with nano-SiO2 and micro-SiO2 investigated by experimental design, Constr. Build. Mater. 24 (2010) 1432–1437, https://doi.org/10.1016/j.conbuildmat.2010.01.012.

[9] L. Zhang, N. Ma, Y. Wang, B. Han, X. Cui, X. Yu, J. Ou, Study on the reinforcing mechanisms of nano silica to cement-based materials with theoretical calculation and experimental evidence, J. Compos. Mater. 50 (2016) 4135–4146, https://doi.org/10.1177/0021998316632602.

[10] L.P. Singh, S.R. Karade, S.K. Bhattacharyya, M.M. Yousuf, S. Ahalawat, Beneficial role of nanosilica in cement based materials - a review, Constr. Build. Mater. 47 (2013) 1069–1077, https://doi.org/10.1016/j.conbuildmat.2013.05.052.

[11] A.H. Korayem, N. Tourani, M. Zakertabrizi, A.M. Sabziparvar, W.H. Duan, A review of dispersion of nanoparticles in cementitious matrices: nanoparticle geometry perspective, Constr. Build. Mater. 153 (2017) 346–357, https://doi.org/10.1016/j.conbuildmat.2017.06.164.

[12] S. Kawashima, T.S. Jung-Woo, D. Corr, M.C. Hersam, S.P. Shah, Dispersion of CaCO3 nanoparticles by sonication and surfactant treatment for application in fly ash-cement systems, Mater. Struct. Constr. 47 (2014) 1011–1023, https://doi.org/10.1617/s11527-013-0110-9.

[13] M.S.M. Norhasri, M.S. Hamidah, A.M. Fadzil, Applications of using nano material in concrete: a review, Constr. Build. Mater. 133 (2017) 91–97, https://doi.org/10.1016/j.conbuildmat.2016.12.005.

[14] Y. Reches, K. Thomson, M. Helbing, D.S. Kosson, F. Sanchez, Agglomeration and reactivity of nanoparticles of SiO2, TiO2, Al2O3, Fe2O3, and clays in cement pastes and effects on compressive strength at ambient and elevated temperatures, Constr. Build. Mater. 167 (2018) 860–873, https://doi.org/10.1016/j.conbuildmat.2018.02.032.

[15] F.U.A. Shaikh, S.W.M. Supit, Effects of superplasticizer types and mixing methods of nanoparticles on compressive strengths of cement pastes, J. Mater. Civ. Eng. 28 (2015), 06015008, https://doi.org/10.1061/(ASCE).

[16] P. Hou, J. Qian, X. Cheng, S.P. Shah, Effects of the pozzolanic reactivity of nanoSiO2 on cement-based materials, Cem. Concr. Compos. 55 (2015) 250–258, https://doi.org/10.1016/j.cemconcomp.2014.09.014.

[17] O.A. Mendoza Reales, Y.P. Arias Jaramillo, J.C. Ochoa Botero, C.A. Delgado, J. H. Quintero, R.D. Toledo Filho, Influence of MWCNT/surfactant dispersions on the rheology of Portland cement pastes, Cem. Concr. Res. 107 (2018) 101–109, https://doi.org/10.1016/j.cemconres.2018.02.020.

[18] A.J. Blanch, C.E. Lenehan, J.S. Quinton, Optimizing surfactant concentrations for dispersion of single-walled carbon nanotubes in aqueous solution, J. Phys. Chem. B 114 (2010) 9805–9811, https://doi.org/10.1021/jp104113d.

[19] J. Luo, Z. Duan, H. Li, The influence of surfactants on the applications and materials science processing of multi-walled carbon nanotubes in reinforced cement matrix composites, Phys. Status Solidi Appl. Mater. Sci. 206 (2009) 2783–2790, https://doi.org/10.1002/pssa.200824310.

[20] B.S. Sindu, S. Sasmal, Properties of carbon nanotube reinforced cement composite synthesized using different types of surfactants, Constr. Build. Mater. 155 (2017) 389–399, https://doi.org/10.1016/j.conbuildmat.2017.08.059.

[21] F. Collins, J. Lambert, W.H. Duan, The influences of admixtures on the dispersion, workability, and strength of carbon nanotube-OPC paste mixtures, Cem. Concr. Compos. 34 (2012) 201–207, https://doi.org/10.1016/j.cemconcomp.2011.09.013.

[22] H. Liu, S. Cui, J. Wang, J. Wang, Influence of chemical admixtures on the dispersion of carbon nanotubes in water and cement pastes, IOP Conf. Ser. Mater. Sci. Eng. 182 (2017), 012029, https://doi.org/10.1088/1757-899X/182/1/012029.

[23] Y. Gu, Q. Ran, X. Shu, C. Yu, H. Chang, J. Liu, Synthesis of nanoSiO2 @PCE core-shell nanoparticles and its effect on cement hydration at early age, Constr. Build. Mater. 114 (2016) 673–680, https://doi.org/10.1016/j.conbuildmat.2016.03.093.

[24] P. Feng, H. Chang, X. Liu, S. Ye, X. Shu, Q. Ran, The significance of dispersion of nano-SiO2 on early age hydration of cement pastes, Mater. Des. 186 (2020) 108320, https://doi.org/10.1016/j.matdes.2019.108320.

[25] P. Hou, J. Shi, S. Prabakar, X. Cheng, K. Wang, X. Zhou, S.P. Shah, Effects of mixing sequences of nanosilica on the hydration and hardening properties of cement-based materials, Constr. Build. Mater. 263 (2020) 120226, https://doi.org/10.1016/j.conbuildmat.2020.120226.

[26] S. Parveen, S. Rana, R. Fangueiro, M.C. Paiva, Microstructure and mechanical properties of carbon nanotube reinforced cementitious composites developed using a novel dispersion technique, Cem. Concr. Res. 73 (2015) 215–227, https://doi.org/10.1016/j.cemconres.2015.03.006.

[27] J. Foldyna, V. Foldyna, M. Zeleňák, Dispersion of carbon nanotubes for application in cement composites, Procedia Eng. 149 (2016) 94–99, https://doi.org/10.1016/j.proeng.2016.06.643.

[28] L. Zhao, X. Guo, Y. Liu, C. Ge, Z. Chen, L. Guo, X. Shu, J. Liu, Investigation of dispersion behavior of GO modified by different water reducing agents in cement pore solution, Carbon N. Y. 127 (2018) 255–269, https://doi.org/10.1016/j.carbon.2017.11.016.

[29] S.R.A. Dantas, R. Serafini, R.C. de Oliveira Romano, F. Vittorino, K. Loh, Influence of the nano TiO2 dispersion procedure on fresh and hardened rendering mortar properties, Constr. Build. Mater. 215 (2019) 544–556, https://doi.org/10.1016/j.conbuildmat.2019.04.190.

[30] J. Liu, J. Fu, Y. Yang, C. Gu, Study on dispersion, mechanical and microstructure properties of cement paste incorporating graphene sheets, Constr. Build. Mater. 199 (2019) 1–11, https://doi.org/10.1016/j.conbuildmat.2018.12.006.

[31] C. Stephens, L. Brown, F. Sanchez, Quantification of the re-agglomeration of carbon nanofiber aqueous dispersion in cement pastes and effect on the early age flexural response, Carbon N. Y. 107 (2016) 482–500, https://doi.org/10.1016/j.carbon.2016.05.076.

[32] Y. Sargam, K. Wang, Influence of dispersants and dispersion on properties of nanosilica modified cement-based materials, Cem. Concr. Compos. 118 (2021) 103969, https://doi.org/10.1016/j.cemconcomp.2021.103969.

[33] M.A. Johnson, Detergents: Triton X-100, Tween-20, and More, Mater. Methods. 3 (2013).

[34] T.F. Tadros, Dispersion of Powders in Liquids and Stabilization of Suspensions, Wiley-VCH Verlag & Co, KGaA, Weinheim, Germany, 2012.

[35] J. Israelachvili, Intermolecular and Surface Forces, Elsevier Inc., 2011, https://doi.org/10.1016/C2009-0-21560-1.

[36] ASTM, C150/C150M-18, Standard Specification for Portland Cement, West Conshohocken, PA, 2018, https://doi.org/10.1520/C0150_C0150M-18.

[37] R.K. Goyal, Nanomaterials and Nanocomposites: Synthesis, Properties, Characterization Techniques, and Applications, CRC Press, 2017, https://doi.org/10.1201/9781315153285.

[38] ASTM, C1611, Standard Test Method for Slump Flow of Self-Consolidating Concrete, West Conshohocken, PA, 2018.

[39] ASTM C109, Standard Test Method for Compressive Strength of Hydraulic Cement Mortars (Using 2-in. or [50-mm] Cube Specimens), ASTM International, West Conshohocken, PA, 2016.

[40] Y. Sargam, K. Wang, A. Tsyrenova, S. Jiang, F. Liu, Data for: Effects of anionic and nonionic surfactants on the dispersion and stability of nanoSiO2 in aqueous and cement pore solutions, Mendeley Data. v1 (2020). doi:10.17632/zc77dbjn6x.1.

[41] U. Pair, J.P. Kim, Y.S. Jung, Y.G. Jung, T. Katoh, J.G. Park, V.A. Hackley, The effect of Si dissolution on the stability of silica particles and its influence on chemical mechanical polishing for interlayer dielectrics, J. Korean Phys. Soc. 39 (2001) S201–S204.

[42] H. Maraghechi, F. Rajabipour, C.G. Pantano, W.D. Burgos, Effect of calcium on dissolution and precipitation reactions of amorphous silica at high alkalinity, Cem. Concr. Res. 87 (2016) 1–13, https://doi.org/10.1016/j.cemconres.2016.05.004.

[43] N. Yuichi, K. Masahisa, T. Osamu, C. Tadashi, Dissolution rates of amorphous silica in highly alkaline solution, J. Nucl. Sci. Technol. 37 (2000) 349–357, https://doi.org/10.1080/18811248.2000.9714905.

[44] Y. Zhang, X. Kong, Correlations of the dispersing capability of NSF and PCE types of superplasticizer and their impacts on cement hydration with the adsorption in fresh cement pastes, Cem. Concr. Res. 69 (2015) 1–9, https://doi.org/10.1016/j.cemconres.2014.11.009.

[45] E. Sakai, T. Kasuga, T. Sugiyama, K. Asaga, M. Daimon, Influence of superplasticizers on the hydration of cement and the pore structure of hardened cement, Cem. Concr. Res. 36 (2006) 2049–2053, https://doi.org/10.1016/j.cemconres.2006.08.003.

[46] E. Gallucci, P. Mathur, K. Scrivener, Microstructural development of early age hydration shells around cement grains, Cem. Concr. Res. 40 (2010) 4–13, https://doi.org/10.1016/j.cemconres.2009.09.015.

[47] A. Bazzoni, Study of Early Hydration Mechanisms of Cement by Means of Electron Microscopy, EPFL, 2014.

[48] E. Berodier, K. Scrivener, Understanding the filler effect on the nucleation and growth of C-S-H, J. Am. Ceram. Soc. 97 (2014) 3764–3773, https://doi.org/10.1111/jace.13177.

[49] I.G. Richardson, Tobermorite/jennite- and tobermorite/calcium hydroxide-based models for the structure of C-S-H: applicability to hardened pastes of tricalcium silicate, β-dicalcium silicate, Portland cement, and blends of Portland cement with blast-furnace slag, metakaol, Cem. Concr. Res. 34 (2004) 1733–1777, https://doi.org/10.1016/j.cemconres.2004.05.034.

[50] P.C. Mathur, Study of Cementitious Materials Using Transmission Electron Microscopy, EPFL, 2007.
[51] I.G. Richardson, G.W. Groves, A.R. Brought, C.M. Dobsont, The carbonation of OPC and OPC/silica fume hardened cement pastes in air under conditions of fixed humidity, Adv. Cem. Res. 5 (1993) 81–86.
[52] R.P. Sear, Nucleation: theory and applications to protein solutions and colloidal suspensions, J. PhysicsCondensed Matter. 19 (2007) 28, https://doi.org/10.1088/0953-8984/19/3/033101.
[53] D. Marchon, U. Sulser, A. Eberhardt, R.J. Flatt, Molecular design of comb-shaped polycarboxylate dispersants for environmentally friendly concrete, Soft Matter 9 (2013) 10719, https://doi.org/10.1039/c3sm51030a.
[54] H. Heinz, C. Pramanik, O. Heinz, Y. Ding, R.K. Mishra, D. Marchon, R.J. Flatt, I. Estrela-Lopis, J. Llop, S. Moya, R.F. Ziolo, Nanoparticle decoration with surfactants: molecular interactions, assembly, and applications, Surf. Sci. Rep. 72 (2017) 1–58, https://doi.org/10.1016/j.surfrep.2017.02.001.
[55] F. Winnefeld, S. Becker, J. Pakusch, T. Götz, Effects of the molecular architecture of comb-shaped superplasticizers on their performance in cementitious systems, Cem. Concr. Compos. 29 (2007) 251–262, https://doi.org/10.1016/j.cemconcomp.2006.12.006.